ISSN 0018-151X, High Temperature, 2016, Vol. 54, No. 1, pp. 11–19. © Pleiades Publishing, Ltd., 2016.
Original Russian Text © A.E. Galashev, O.R. Rakhmanova, 2016, published in Teplofizika Vysokikh Temperatur, 2016, Vol. 54, No. 1, pp. 13–22.

PLASMA INVESTIGATIONS

Computer Simulation of a Forced Drift of Lithium Ions through Graphene Membranes

A. E. Galashev and O. R. Rakhmanova

Institute of High Temperature Electrochemistry, Ural Branch, Russian Academy of Sciences, Yekaterinburg, 620137 Russia
e-mail: galashev@ihte.uran.ru

Received September 2, 2014

Abstract—A drift of Li^+ ions upon electric interactions in a planar channel formed by graphene sheets and a cell separated by two graphene membranes with pores of various types has been investigated by the molecular dynamics method. The optimal size of the planar channel gap is determined based on the character of the ion dynamics and the ion effect on the physical properties of the graphene sheets. A set of graphene sheets with divacancies demonstrates the best throughput of lithium ions among six sets of membrane pairs. The ions passing through the membrane are found to affect the kinetic characteristics of the graphene membranes.

DOI: 10.1134/S0018151X15050120

INTRODUCTION

Currently, questions of mass transfer in a porous medium are of great importance for the intensively developing energy-saving systems of the next generation. The molecular-dynamic (MD) simulation performed on three-dimensional unit cells with periodic boundary conditions for a combined system, which is an anode–electrolyte–cathode material, yielded diffusion coefficients of lithium ions in the solid carbon phase in the range from 10^{-10} to 10^{-9} cm^2/s [1]. The presence of bent channels in the modeled amorphous carbon phase slows down the lithium ion diffusion and increases the capacity of a lithium battery (in comparison with that of a graphite-based battery).

Graphite materials, which are traditionally used as electrodes in lithium-ion batteries, provide a small capacity due to the limited number of storage sites of Li ions in the sp^2 hexagonal structure [2]. The theoretical specific graphite capacity (which can be obtained by forming interstitial compounds LiC_6) is 372 mA h g^{-1} [3]. Graphite is a widespread anode material for Li batteries because of its high Coulomb efficiency and cycle stability [3]. Therefore, the anode used in most lithium-ion accumulators is based on graphite, the interlayer space of which contains up to one Li^+ ion for every six carbon atoms [4]. The energy density of a lithium-ion accumulator cannot meet the demands of portable electronic devices due to the power limit determined by graphite. If graphite could be replaced by graphene, the expected carbon-material capacity increases to 500–1100 mA h g^{-1}. It was established in [5] by the quantum molecular dynamics method that the electron–hole plasma of the carbon electrode affects the system capacity significantly.

The specific characteristics of graphene are inherited in its peculiar structure, in which a Li atom or ion is located in the surface and edge regions [6]. During intercalation, Li transfers its 2*s* electron to carbon atoms, where it would be between carbon sheets. The high capacity of two-dimensional carbon material provides the possibility for incorporating lithium into "depressions" on the material plane [7], adsorbing lithium on each side of the carbon sheet [8], binding lithium by the so-called "covalent" bond [7], and binding lithium at hydrogenated edges of graphene fragments [9, 10]. Lithium ions can be adsorbed on both sides of graphene sheets that are stacked like a house of cards, which leads to two lithium layers for each graphene sheet with a theoretical power of 744 mA h g^{-1} due to the formation of $Li_{12}C_6$ [7, 11, 12]. The charge/discharge cycles (with a capacity of 540 mA h g^{-1} in the first cycle) in graphene nanosheets filled with Li were described in [13, 14]. The capacity of graphene doped with Li^+ in order to store hydrogen was also considered [15–18]. There have been attempts to change the structure of the Li-adsorbing layers with the aim of adsorbing more Li atoms [6]. The interaction between Li^+ and the graphite surface was studied theoretically using small carbon clusters for lithium adsorption. In the case where the covalent bond is formed in the disordered carbon by a benzene ring, the predicted capacity was as high as 1116 mA h g^{-1} [3]. Calculations of the binding energy between Li^+ and the $C_{32}H_{18}$ cluster, performed using the density functional theory, showed that the Li^+ ion is mainly bound with the cluster edges [19]. Li^+-containing edges of the C_{96} cluster are more stable than its major part [20]. The minimum spacing between the graphene sheets, which provide movement of a Li^+ ion and, accordingly, an increase in

the alkaline-battery capacity, was estimated in [21]. This spacing was obtained based on a static model with the Lennard-Jones (LJ) Li–C interaction to be 5 Å.

The purpose of this study is to analyze the possibility of using defect graphene as anode elements for lithium-ion batteries based on propagation of lithium ions through paired graphene sheets by means of monovacancies, divacancies, trivacancies, and hexavacancies.

1. COMPUTER MODEL

In the first part of this study, we determine the interplanar spacing h at which the Li^+ ion incorporated between two graphene sheets can be displaced in the dynamic model. The molecular-dynamic calculations were performed with the values $h = 5.0$, 5.5, 6.0, and 6.5 Å. The first value coincides with the corresponding parameter obtained in the static model [21]. To compare the results of the mechanical effect of the ion moving in a dc electric field on the graphene sheets forming the planar channel, the ion was initially placed into the channel at a distance $\sigma_{Li-C}^{LJ} = 2.473$ Å (σ_{Li-C}^{LJ} is the LJ potential parameter) from the front boundary of the slit (the plane oriented perpendicular to the *ox* direction). When the Li^+ ion is initially at the same distance before the front boundary of the slit (i.e., beyond the channel), it cannot enter this channel under the field with a strength of 10^3 V/m, tracing loops in front of its inlet.

In the second part of this study, we report the results of simulating the charge cycle of an alkaline battery, which contains two parallel sheets of defect graphene. In this case, the defects are monovacancies, divacancies, and trivacancies (nine of each per sheet), as well as hexavacancies (six per sheet composed of 406 C atoms). The defects in each graphene sheet are described by an approximately uniform regular distribution. However, for adjacent graphene sheets, defects are continuously shifted, thus hindering direct propagation of Li^+ ions through the adjacent sheets.

At the initial instant, the lower part of the cell was filled with ten Li^+ ions by a random-number generator; each ion had an electric charge of $+1.0e$, where e is the elementary charge. The directed ion motion (upwards) was provided by a positive electric charge of $+10e$ of the lower cell base and a negative charge of $-10e$ of the upper base. Each of these charges was formed by ten identical point charges. This virtual capacitor affected the model cell for the first four million time steps $\Delta t = 2 \times 10^{-16}$ s. This process will be referred to as "charging." To enhance chaotization of ion movement throughout the cell, we applied the effect of random-walking electric charges (positive at the lower cell base and negative at the upper base). The random charge walk over the model-cell bases was achieved by a random-number generator changing the charge positions at each time step. After four million time steps, the Li^+ ions that reached the upper cell base lost their electric charges. Afterwards, the dc electric field of 10^3 V/m moved Li^+ ions in the reverse direction in the absence of electric charges at the cell end faces in eight million time steps ("discharging").

The detailed description of the interactions in graphene is based on the widespread Tersoff potential [22], which, however, like the more modern REBO potential, cannot adequately demostrate chemical reactions in various media [23]. The Tersoff potential is based on the concept of bond order. The potential energy between two neighboring atoms i and j can be written as

$$V_{ij} = f_C(r_{ij})\left[A\exp(-\lambda^{(1)}r_{ij}) - Bb_{ij}\exp(-\lambda^{(2)}r_{ij})\right],$$

$$f_C(r_{ij}) = \begin{cases} 1, & r_{ij} < R^{(1)}, \\ \frac{1}{2} + \frac{1}{2}\cos\left[\pi(r_{ij} - R^{(1)})/(R^{(2)} - R^{(1)})\right], & \\ R^{(1)} < r_{ij} < R^{(2)}, & \\ 0, & r_{ij} > R^{(2)}, \end{cases}$$

where b_{ij} is the multiparticle bond-order parameter describing how the bond-formation energy is generated (attractive part of V_{ij}) in the local atomic arrangement due to the presence of other neighboring atoms. The potential energy is a multiparticle function of the positions of atoms i, j, and k and is determined by the parameters

$$b_{ij} = (1 + \beta^n \xi_{ij}^{n_i})^{-1/(2n)},$$

$$\xi_{ij} = \sum_{k \neq i,j} f_C(r_{ij}) g(\theta_{ijk}),$$

$$g(\theta_{ijk}) = 1 + \frac{c^2}{d^2} - \frac{c^2}{\left[d^2 + (h - \cos\theta_{ijk})^2\right]}.$$

Here, ξ is the effective coordination number and $g(\theta_{ijk})$ is the function of the angle between r_{ij} and r_{ik}, which stabilizes the tetrahedral structure. The Tersoff potential parameters for carbon were mainly taken from [22]; however, the covalent binding distance was increased to 0.23 nm, and an additional weak attraction was introduced at $r > 0.23$ nm, which is set by the LJ potential with the parameters of [24]. To eliminate the resulting torque, the rotational component of the force formed by atoms in adjacent sites was excluded at each site of the graphene sheet. The analytical form of the local torsional interaction potential was given in [24]. The Li^+–C interaction was simulated using the conventional LJ potential with the parameters of [21].

The concentration sites of C atoms with dangling bonds (i.e., atoms around a vacancy and atoms at the graphene-sheet edges) were subjected to hydrogen physiosorption. In this case, C atoms forming vacancies are of particular interest. The stable position of the H atom under physiosorption is known to be above a C atom at a distance of $r_{CH} = 1.13$ Å [25]. C atoms, which neighbor H atoms, also exhibit an increase in the

Table 1. Parameters of the Tersoff (for carbon) and Lennard-Jones potentials and the value and number of charges in the system

Parameters	Carbon	Interactions	σ, Å	ε, eV
A, eV	1.3936×10^3	C–C	3.400	0.00284
B, eV	3.4674×10^2	Li–Li	1.506	0.71597
$\lambda^{(1)}$, Å^{-1}	3.4879	Li–C	2.473	0.00433
$\lambda^{(2)}$, Å^{-1}	2.2119	Li–CH	2.638	0.05327
β	1.5724×10^{-7}	C–CH	3.535	0.04554
n	7.2751×10^{-1}	CH–CH	3.7700	0.00396
c	3.8049×10^4	Charges	Charge value, e	Charge number
d	4.384	$q_{Li^+}(q_{Li})$	+1(0)	10
h	–0.57058	q_{lb}	+1	10
$R^{(1)}$, Å	1.8	q_{hb}	–1	10
$R^{(2)}$, Å	2.3	q_{CH}	0º+0.35	54–90
–	–	q_{Cpore}	–0.35–0	54–90

interatomic spacing r_{CC} from 1.415 Å (before hydration) to 1.485 Å (after hydration). The CH groups formed around a vacancy will be considered within the united scheme. This scheme was studied well in the molecular simulation when developing transferred force fields used for predicting the thermodynamic properties of complex molecules [26, 27]. The interaction between CH groups was performed through the LJ potential with the parameters of [28]. The interaction between Li^+ ions and CH groups (as well as between Li^+ ions) was determined by the LJ and Coulomb contributions. There is also the LJ interaction between Li^+ ions and C atoms, the parameters of which were determined in [21]. The Berthelot–Lorenz rule was used to determine the LJ parameters of C–CH and Li^+–CH interactions.

Propagation of Li^+ ions through pores in the membranes was specially controlled. An ion was allowed to cross the membrane only at the point (on its plane) that falls in the circle of the effective radius of a particular pore. The presence of fractional electric charges at the pore perimeters facilitated the reaching of pores by ions. The charges were assigned to both CH bonds and the same number of randomly chosen free atoms at the pore boundaries. The number of CH bonds corresponded to that of the nearest neighbors (among C atoms) to the pore center. For example, the number of these bonds was three for monovacancies, four for divacancies, five for trivacancies, and six for hexavacancies. The CH group was described according to the united atom scheme [28]. The positive charges of CH groups and negative charges of hydrogen-free C atoms at the pore edges had a fluctuating nature and were set by the random-number generator. The maximum charge for the CH group (+0.35e) formed a Coulomb potential for the Li^+ ion motion, which corresponded to the value of the energy barrier for Li atom diffusion on the graphene sheet by vertices of C atoms [29]. The calculations performed by the method of the density functional theory indicate alternating fluctuation in the charge value of atoms located in the vicinity of graphene-sheet pores [30]. The fluctuating charges q_{CH} (CH groups) and q_{Cpore} (C atoms) in our model varied in the range $-0.35e \le q_{CH} \le 0.35e$. The parameters of all potentials used and the values and numbers of charges present in the system are listed in Table 1.

The temperature in the model was maintained constant by applying a Berendsen thermostat with the bonding constant $\tau = 4$ fs [31]. The maintained temperature did not correspond to the specified one (300 K) because of the slow kinetic-energy exchange. The Li^+ ion motion in the planar channel was simulated with mobile C atoms in the graphene sheets. The simulation of lithium-ion propagation through the graphene membranes was performed with immobile C atoms. This approximation could not affect significantly the final result due to the high rigidness of C–C bonds and, at the same time, made it possible to reduce significantly the calculation time, which was ~78 h. Since the diffusion of Li^+ ions is too slow, their percolation through the porous medium was not directly investigated in the molecular-dynamics simulation of the system with the "anode–electrolyte–cathode" structure [1].

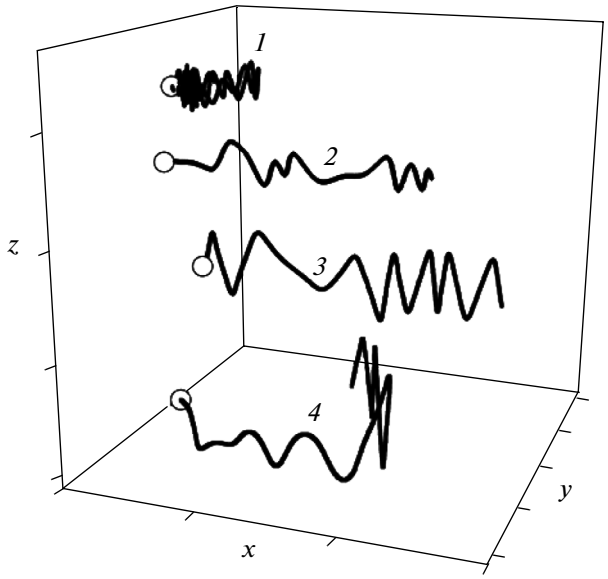

Fig. 1. Trajectories of lithium ion motion in a planar graphene channel with a gap: (*1*) 5.0, (*2*) 5.5, (*3*) 6.0, and (*4*) 6.5 Å.

The self-diffusion coefficient is calculated through the mean-square atomic displacement $\left\langle\left[\Delta\mathbf{r}(t)\right]^2\right\rangle$ [25]

$$D = D_{xy} + D_z = \lim_{t\to\infty}\frac{1}{2\Gamma t}\left\langle\left[\Delta\mathbf{r}(t)\right]^2\right\rangle_n,$$

where $\Gamma = 3$ is the space dimension. The time averaging is denoted as $\langle\ldots\rangle$, and n is the number of time intervals for determining $\left\langle\left[\Delta\mathbf{r}(t)\right]^2\right\rangle$. Here, the time mean was determined by averaging 20 curves, each of which was calculated in a 40-ps interval (or $200000\Delta t$). Transition to the limit $t \to \infty$ is impossible for MD models; however, this transition is not necessary because random walks are limited by the system size L and the probability that the random-walk distance exceeds L is on the order of the $L/(\bar{v}\sqrt{t})$ value ($\bar{v}$ is the mean particle velocity in the system) [32]. In the case of "charging," $t = 800$ ps; therefore, the hypothetical probability of this event is ≈0.001. The D value is generally averaged over time intervals including many collisions (up to several hundred).

To calculate stresses arising from the Li^+ ion motion in graphene, the graphene sheet was divided into elementary areas. These stresses were calculated taking into account only the contributions due to Li^+–C interactions. The atomic stresses $\sigma_J^i(l)$ in the elementary area with the number l for each direction x, y, and z with the current index J are determined by calculating the kinetic energies of atoms in this area and the projections of forces f_J^i exerted on the lth area from all other atoms:

$$\sigma_J^i(l) = \left\langle\sum_i^k\frac{1}{\Omega}\left(mv_J^iv_J^i\right)\right\rangle + \frac{1}{S_l}\left\langle\sum_i^k\left(f_J^i\right)\right\rangle,$$

where k is the number of atoms in the lth area, Ω is the volume per atom, m is the atomic mass, v_J^i is the J velocity projection of the ith atom, and S_l is the lth area. The compressive stresses thus determined can have a sign of either "+" or "–", according to the directions of forces f_J^i. This is the difference in the microscopic stress $\sigma_J^i(l)$ and the macroscopic stress $\bar{\sigma}_J < 0$.

The total energy of a free single sheet of graphene was obtained at $T = 300$ K to be –7.02 eV, which is in agreement with the quantum-mechanical calculation (–6.98 eV) [33]. It is known that a neutral lithium atom is adsorbed in the vicinity of a vacancy on graphene binding with the surface with even higher energy as compared with the lithium cohesion energy (0.36 eV/atom). The binding energy of atomic hydrogen with defect graphene was calculated within the theory of the density functional to be 0.875 eV/atom [34]. The estimated binding energy of the Li atom with graphene containing divacancies was obtained in an individual MD calculation to be ~0.4 eV/atom. An alternating fluctuating charge near pores on graphene allows lithium ions to overcome this energy barrier and not be retarded near defects.

2. CALCULATION RESULTS

The trajectories of a Li^+ ion, preliminarily placed into the channel formed between the graphene planes and propagating under a dc electric field of 10^3 V/m, are shown in Fig. 1. The initial trajectory point is arbitrarily indicated by a circle. At the minimum gap (5.0 Å), the ion moves along the field for a very short distance. Its trajectory has the form of a quasi-sinusoid with a small oscillation amplitude. The oscillation amplitude is restricted by the graphene sheets forming the planar channel. At the gap of 5.5 Å, the Li^+ ion placed into the channel passes a rather large distance (~15 Å) with small transverse aperiodic oscillations; nevertheless, it is trapped in the gap being significantly slowed down by the graphene planes. A larger increase in the gap (to 6.0 Å) allows for ion propagation through the entire channel. Aperiodic oscillations, the frequency of which increases while approaching the channel output, are imposed on the ion translational motion. The amplitude of these oscillations is much larger than that in the previous case. Finally, the ion leaves the channel. A further expansion of the gap (to 6.5 Å) changes significantly the propagation trajectory of the Li^+ ion along the channel. Undergoing aperiodic oscillations, the ion moves along the channel only to a certain point, where its trajectory makes a sharp turn, and the subsequent oscillating ion motion occurs in the direction that only slightly deviates from the

graphene-sheet diagonal. For efficient control of the ion motion along the channel applying a dc electric field of 10^3 V/m, it is most expedient to choose the gap between graphene sheets to be 6.0 Å.

The MD simulation of heating metal (Al, Ni) films on two-layer graphene revealed an increase (related to the increase in temperature) in the mobility of C atoms during vertical displacements in one graphene sheet due to a decrease in the corresponding mobility in the other sheet [35, 36]. Thus, the presence of metal binds the dynamics of atoms in parallel graphene sheets. Therefore, one might expect that the presence of a Li^+ ion in the planar channel would also affect significantly the dynamic and mechanical properties of graphene sheets forming this channel.

The horizontal (D_{xy}) and vertical (D_z) mobilities of C atoms in the lower (*1*) and upper (*2*) graphene sheets are shown in Fig. 2 for different h values. At the gap $h = 5.5$ Å, the smallest D_{xy} value can be observed in the upper sheet, which is compensated by the largest (among the presented) D_z value. Against the background of significant variations in the D_{xy} and D_z values for the upper sheet, the change in these characteristics for the lower sheet appears insignificant. It is noteworthy that the D_{xy} and D_z values for the gap of 6.0 Å are comparable with similar characteristics at $h = 5.0$ Å; in half of the cases, these values are even smaller, although displacements of the Li^+ ion along the channel differ sharply for these gaps.

The partition of the graphene sheets into areas containing atomic rows in the "armchair" direction makes it possible to consider the distribution of stress tensor components in the "zigzag" direction in graphene. When a Li^+ ion propagates along the channel, the most significant stress tensor component in the graphene-sheet plane is σ_{zz} determined by vertically directed forces. For two-layer graphene in a vacuum, the function $\sigma_{zz}(x)$ has an oscillation amplitude no larger than ±50 GPa [35, 36]. When a Li^+ ion moves between the graphene sheets, the oscillation amplitude of the function $\sigma_{zz}(x)$ may be several times larger than this value (Fig. 3). An especially strong fluctuation in the σ_{zz} value is observed at the gap of 5.5 Å in the vicinity of the value $x = 1.1$ nm (curve *2*). The strongest fluctuations for other h values are characterized by fairly close values, which are much smaller as compared with the case of $h = 5.5$ Å. The highest total stress σ_{zz} in graphene (−1.03 GPa) was obtained at $h = 5.5$ Å; this value falls in the relaxation range of the corresponding stress (−3...+1.8 GPa) formed upon deflection of a graphene ribbon [37]. Thus, with regard to propagation of the largest distance by a Li^+ ion with a minimum influence on the physical properties of graphene sheets, a gap of 6.0 Å appears most acceptable.

Specifically this gap between the graphene sheets was chosen for simulating Li^+ ion motion through

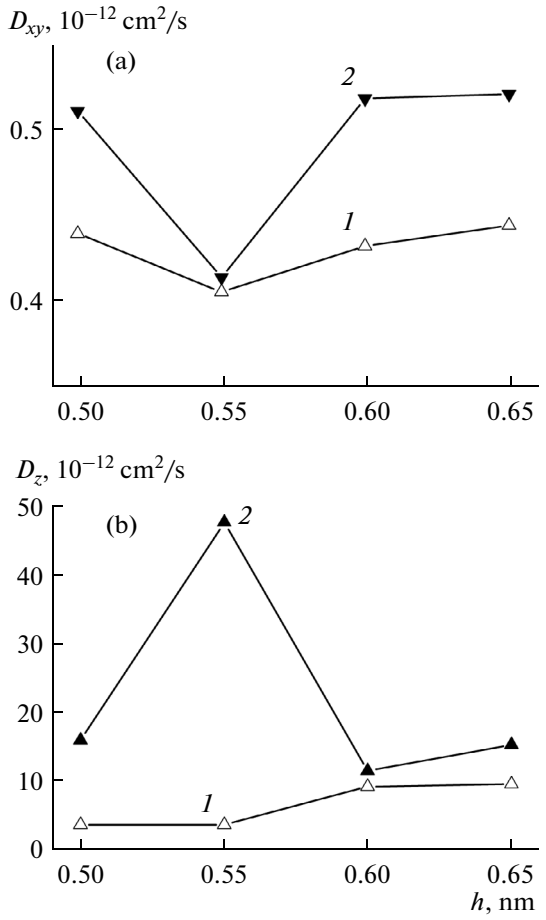

Fig. 2. Coefficients of the (a) horizontal and (b) vertical mobility of graphene atoms in the (*1*) lower and (*2*) upper sheets forming the planar channel. The lithium ion begins to move inside the channel.

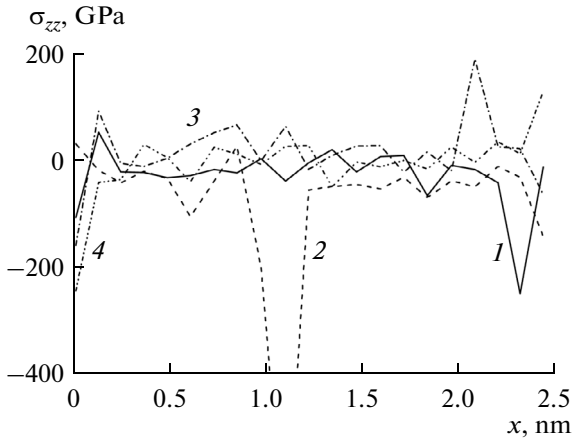

Fig. 3. Distribution of the stress $\sigma_{zz}(x)$, averaged over both graphene sheets, along the *ox* axis ("zigzag" direction) coinciding with the direction of the electric field strength for different gaps: (*1*) 5.0, (*2*) 5.5, (*3*) 6.0, and (*4*) 6.5 Å.

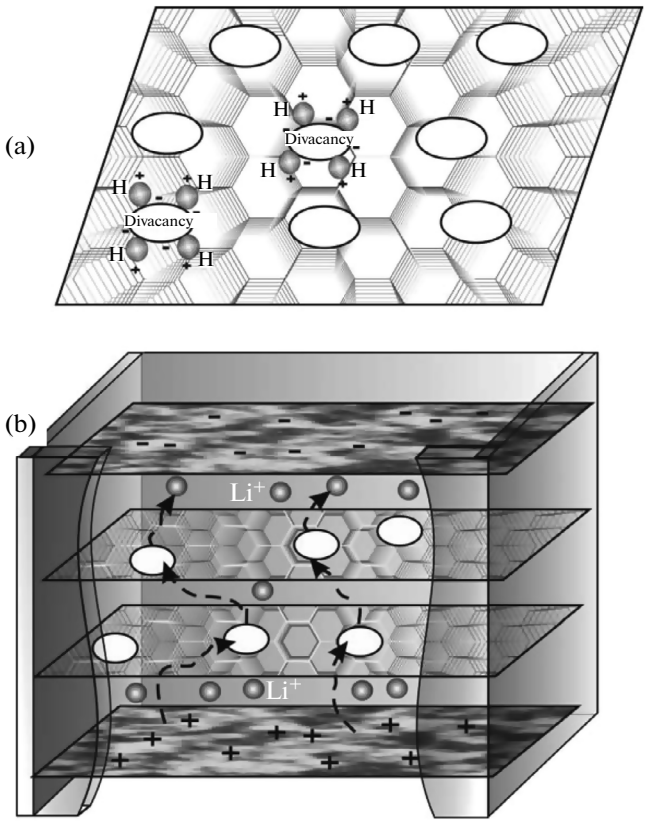

Fig. 4. Schematics of the (a) membrane and (b) basic cell: (H) CH groups represented by the united atom scheme; C atoms are omitted; ellipses indicate divacancies; signs "+" and "–" are positive and negative charges; and the arrows show Li^+ ion drift.

porous membranes. The basic-cell diagram is shown in Fig. 4. One of the graphene membranes used is shown schematically, with C atoms not highlighted, at the top. The pores in the upper membrane are shifted by a distance no larger than the graphene lattice period to avoid direct vertical propagation of the Li^+ ion through two membranes at once. The lower and upper membranes could be of either identical or different type. The numbers of basic cells, differing in the type of membranes used, and the steady-state temperatures in the model are given in Table 2. Thus, each of six basic cells was divided into three chambers with identical heights (0.6 nm): lower, intermediate (enclosed between graphene membranes), and upper.

The MD method retains the Newtonian dynamics only for times shorter than t_m^d, where t_m^d determines the time interval in which the solution to the system of Newtonian equations for equilibrium systems is close to the exact one [38]. The estimation of t_m^d from the behavior of the velocity autocorrelation function [38] yields the value 10–15 ps, which is much smaller than the total "charge" time (800 ps). Therefore, the behavior of Li^+ ions during the observation time is affected to a great extent by stochastic correlations. The stochastization is enhanced in the presence of fluctuating charges both on the basis of the basic cell and in the vicinity of membrane pores. This makes the method used closer to the Monte Carlo method and allows one to obtain the pattern of ion diffusion through the porous medium. The system analyzed in this study is not isolated, and the total energy is not conserved in it.

The best result of Li^+ ion propagation through the membranes was achieved in version 4. In this case, nine of ten ions reached the upper cell base after four million time steps; one ion was stopped by the lower membrane within the same time. In the worst case, version 2, after four million time steps, six Li^+ ions are found directly near the upper cell base, one ion has just penetrated through a pore of the second (upper) membrane, two ions have passed the first membrane, and one more ion still remains in the lower cell chamber (Fig. 5). In the other cases, there are seven Li^+ ions in the upper chamber by the end of the "charge" process, and the largest number of ions (two) remain in the lower chamber in version 1 of the membrane set. The

Table 2. Versions of a membrane set in the basic cell (types and number of vacancies and number of C atoms in the lower and upper membranes) and stationary temperatures

Versions	1	2	3	4	5	6
Type and number of pores in the lower membrane	monovacancies 9	divacancies 9	trivacancies 9	divacancies 9	trivacancies 9	hexavacancies 6
Type and number of pores in the upper membrane	divacancies 9	trivacancies 9	hexavacancies 6	divacancies 9	trivacancies 9	hexavacancies 6
Number of C atoms in the lower membrane	397	388	379	388	379	370
Number of C atoms in the upper membrane	388	379	370	388	379	370
T, K	311.5	312.5	312.8	311.6	313.9	298.8

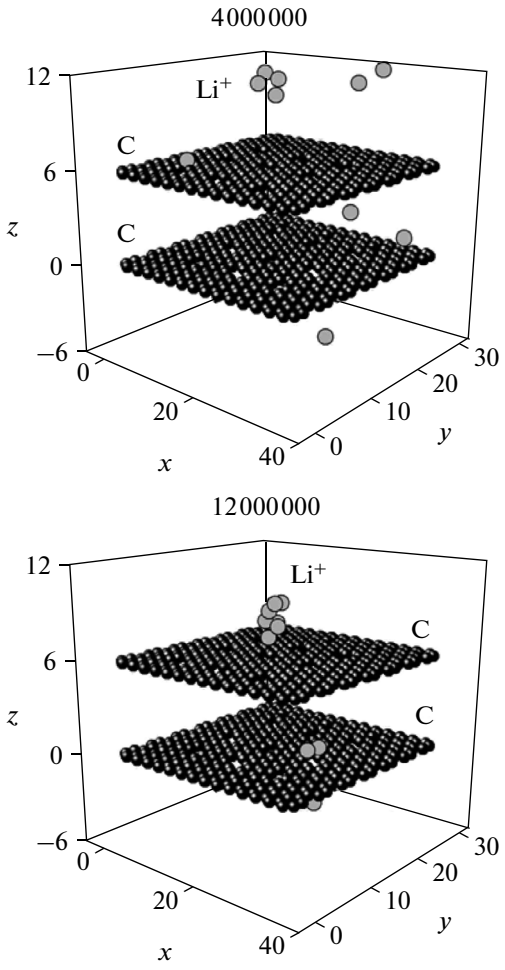

Fig. 5. Basic cell with the membrane set of version 2 at the instants corresponding to 4 and 12 million time steps (the atomic coordinates are in angstroms).

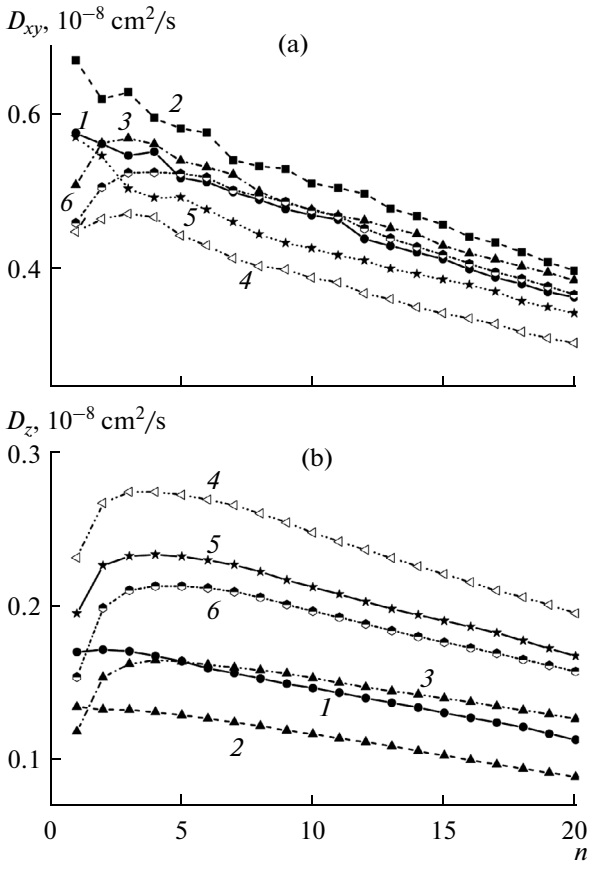

Fig. 6. (a) Horizontal and (b) vertical components of the Li^+ ion mobility coefficient for versions *1*–*6* of the membrane sets listed in Table 2.

latter fact can be explained by the difficulties in propagation of Li^+ ions through monovacancies.

The mobility coefficients of Li^+ ions in both the horizontal (D_{xy}) and vertical (D_z) directions have a tendency to decrease after the first million time steps of the "charge" process or $n = 5$ (Fig. 6). Note that the interval values of D_{xy} and D_z change at an even higher rate. However, at the initial stage of "charging," the coefficient D_{xy} can either increase or decrease for different combination versions of graphene membranes (Fig. 6a), whereas the coefficient D_z at this stage of "charging" increases in four of six cases. Only version 2 exhibits a stable decrease in the D_z value, and a weak short-term increase in this coefficient is observed in the initial calculation stage for version 1. Obviously, the initial rise in the coefficients D_{xy} and D_z is related to the fact that ions acquire certain energy because of mutual repulsion and to expansion of the migration volume due to their ability of passing through membranes. The subsequent stable decrease in these coefficients is caused by a gradual reduction of the available-for-migration volume due to the approach of ions to the upper cell base and the low probability of their motion in the reverse direction. The largest D_{xy} values and the smallest D_z values were revealed for the system with the membrane set of version 2. Here, the highest mobility of Li^+ ions in the horizontal directions is combined with the lowest mobility in the vertical direction. The antipode of this version is version 4, where the minimum ion mobility in the horizontal directions is compensated by the highest mobility in the direction oriented perpendicular to the membrane plane. The mutual compensation of D_{xy} and D_z values is also observed for the other versions of membrane combination.

The relationship between the throughputs of the membrane sets used is also confirmed by the time dependence of the mean level $z_{\text{lev}} = \frac{1}{n_i}\sum_i^{n_i} z_i$ (where z_i is the ion coordinate and n_i is the number of ions) of the lift of Li^+ ions in the system (Fig. 7). Here, the highest mean lift of ions in the cell was detected for the

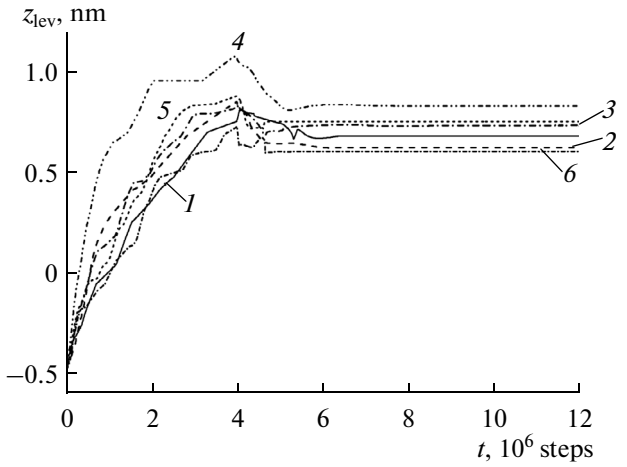

Fig. 7. Mean lift level of Li^+ ions in the basic cell for versions *1–6* of the graphene membrane sets.

membranes of version 4, while the lowest one was observed for versions 6, 2, and 1. In all cases, the highest point of the ion lift is in the vicinity of the end of the "charge" time (i.e., four million time steps). Having reached the upper, negatively charged plate of the external "capacitor," positively charged lithium ions should be electrically neutralized due to the charge flow. Therefore, the contact with the upper wall of the basic cell was accompanied by removal of the electric charge from the ion. The "charging" end in the model indicated the cessation of the virtual external "capacitor." The "charging" is feasible when the external "capacitor" is used and unfeasible when the dc electric field with strengths of 10^3 and 10^4 V/m is applied. In this case, ions remained in the lower chamber near its walls rather than moving upwards through the membranes. The "discharge" process began with switching on the dc electric field $E = 10^3$ V/m inducing the reverse ion motion. It is noteworthy that, after the ions that reached the upper cell base lost the electric charge and acquired the status of atoms, at the same time they inherited the tendency of cluster formation. In all cases without exception, Li atoms in the upper chamber were agglomerated into clusters after 12 million time steps (Fig. 5), which made it impossible for them to pass through the upper membrane in the reverse direction (downwards). The formed clusters always had contact with graphene. During the "discharging," a rather rapid (within 1.8 million time steps) and small decrease in the z_{lev} value was observed. Two million steps after the end of the "charging," the dependence $z_{lev}(t)$ is shown by horizontal portions in all the cases under consideration. This is due to cluster formation by Li atoms in the upper cell chamber and the Li^+ ion adhesion to the graphene surface.

CONCLUSIONS

The behavior of a lithium ion in a planar channel formed by graphene sheets under a dc longitudinal electric field was investigated. The elements of the basic-cell model were tested in individual calculations. Their energy characteristics and mechanical properties correspond to the experimental and MD data of other studies and to the calculation results according to the density functional theory. Characteristic changes in graphene that accompany ion movement were established. The membrane pair that is most efficient for ion propagation among the six investigated versions was formed by two identical graphene sheets with divacancies. The close-to-uniform arrangement of divacancies in each sheet had a shift of ~0.14 nm to prevent ion propagation through two membranes at once. The loss of electric charge by Li^+ ions leads to the formation of a lithium cluster which is insensitive to the electrostatic directing force. In addition, in the dc electric field Li^+ ions "adhere" to the membranes due to the high adhesive ability of graphene. These factors hinder the "discharging" process of the device considered. Ions have very short trajectories of the reverse motion. During the "charging" period, Li^+ ions have the lowest mobility in the horizontal directions and the highest mobility in the vertical direction in the case of an efficient transmission membrane pair. For inefficient membrane pairs, the situation is the opposite. The mean level of vertical ion displacements in the system can also yield an objective estimate of the efficiency of the membrane pairs used. Its time dependence makes it possible to determine the degree and duration of "charging."

The studied devices can find an application not only for developing graphene anodes for lithium batteries but also in biological experiments. For example, they can be used to determine the length of a DNA molecule and identify sequences of molecular pairs in it.

REFERENCES

1. Marquez, A., *Mater. Chem. Phys.*, 2007, vol. 104, p. 199.
2. Sato, K., Noguchi, M., Demachi, A., Oki, N., and Endo, M., *Science* (Washington), 1994, vol. 264, p. 556.
3. Tarascon, J.M. and Armand, M., *Nature* (London), 2001, vol. 414, p. 359.
4. Lian, P., Zhu, X., Liang, S., Li, Z., Yang, W., and Wang, H., *Electrochim. Acta*, 2010, vol. 55, p. 3909.
5. Lankin, A.V., Norman, G.E., and Stegailov, V.V., *High Temp.*, 2010, vol. 48, no. 6, p. 837.
6. Kurita, N. and Endo, M., *Carbon*, 2002, vol. 40, p. 253.
7. Wang, G., Shen, X., Yao, J., and Park, J., *Carbon*, 2009, vol. 47, p. 2049.
8. Dahn, J.R., Zheng, T., Liu, Y.H., and Xue, J.S., *Science* (Washington), 1995, vol. 270, p. 590.
9. Liu, Y.H., Xue, J.S., Zheng, T., and Dahn, J.R., *Carbon* (Washington), 1996, vol. 34, p. 193.

10. Tachikawa, H. and Shimizu, A., *J. Phys. Chem. B*, 2005, vol. 110, p. 20445.
11. Novoselov, K.S., Geim, A.K., Morozov, S.V., Zhang, Y., Dubonos, S.V., Grigorieva, I.V., and Firsov, A.A., *Science* (London), 2004, vol. 306, p. 666.
12. Lin, C.A., Liedl, T., Sperling, R.A., Fernández-Argüelles, M.T., Costa-Fernández, J.M., and Pereiro, R., *J. Mater. Chem.*, 2007, vol. 17, p. 1343.
13. Yoo, E.J., Kim, J., Hosono, E., Zhou, H.S., Kudo, T., and Honma, I., *Nano Lett.*, 2008, vol. 8, p. 2277.
14. Wang, G., Wang, B., Wang, X., Park, J., Dou, S., Ahn, H., and Kim, K., *J. Mater. Chem.*, 2009, vol. 19, p. 8378.
15. Wang, D., Kou, R., Choi, D., Yang, Z., Nie, Z., Li, J., Saraf, L.V., Hu, D., Zhang, J., Graff, G.L., Liu, J., Pope, M.A. and Aksay, I.A., *ACS Nano*, 2010, vol. 4, p. 1587.
16. Winter, M. and Broad, R.J., *Chem. Rev.*, 2005, vol. 105, p. 1021.
17. Brouce, P.G., Scrosati, B., and Tarascon, J.M., *Angew. Chem., Int. Ed.*, 2008, vol. 47, p. 2930.
18. Walkihara, M., *Mater. Sci. Eng., R*, 2001, vol. 33, p. 109.
19. Marquez, A., Vargas, A., and Balbuena, P.B., *J. Electrochem. Soc.*, 1998, vol. 145, p. 3328.
20. Nakadaira M., Saito R., Kimura T., Dresselhaus G., and Dresselhaus, M.S., *J. Mater. Res.*, 1997, vol. 12, p. 1367.
21. Chan, Y. and Hill, J.M., *Micro Nano Lett.*, 2010, vol. 5, p. 247.
22. Tersoff, J., *Phys. Rev. Lett.*, 1988, vol. 61, p. 2879.
23. Orekhov, N.D. and Stegailov, V.V., *High Temp.*, 2014, vol. 52, no. 2, p. 198.
24. Stuart, S.J., Tutein, A.V., and Harrison, J.A., *J. Chem. Phys.*, 2000, vol. 112, p. 6472.
25. Rangel, E., Vazquez, G., and Magana, F., *J. Mol. Model.*, 2012, vol. 18, p. 5029.
26. Poncela, A., Rubio, A.M., and Freire, J.J., *Mol. Phys.*, 1997, vol. 91, p. 189.
27. Wick, C.D., Martin, M.G., and Siepmann, J.I., *J. Phys. Chem. B*, 2000, vol. 104, p. 8008.
28. Lamari, F.D. and Levesque, D., *Carbon*, 2011, vol. 49, p. 5196.
29. Ataca, C., Akturk, E., Ciraci, S., and Ustunel, H., *Appl. Phys. Lett.*, 2008, vol. 93, p. 043123.
30. Kheirabadi, N. and Shafiekhani, A., *Physica E* (Amsterdam), 2013, vol. 47, p. 309.
31. Berendsen, H.J.C., Postma, J.P.M., van Gunsteren, W.F., DiNola, A., and Haak, J.R., *J. Chem. Phys.*, 1984, vol. 81, p. 3684.
32. Kuksin, A.Y., Morozov, I.V., Norman, G.E., Stegailov, V.V., and Valuev, I.A., *Mol. Simul.*, 2005, vol. 31, p. 1005.
33. Davydov, S.Yu., *Phys. Solid State*, 2012, vol. 54 no. 4, p. 875.
34. Rangel, E., Ramírez-Arellano, J.M., Carrillo, I., and Magana, L.F., *Int. J. Hydrogen Energy*, 2011, vol. 36, p. 3657.
35. Galashev, A.E. and Rakhmanova, O.R., *High Temp.*, 2014, vol. 52, no. 3, p. 374.
36. Galashev, A.E., *High Temp.*, 2014, vol. 52, no. 5, p. 633.
37. Neek-Amal, M. and Peeters, F.M., *Appl. Phys. Lett.*, 2010, vol. 97, p. 153118.
38. Norman, G.E. and Stegailov, V.V., *Mat. Model.*, 2012, vol. 24, no. 6, p. 3.

Translated by A. Sin'kov